When local deformations trigger lattice instability: Flow diagram investigations for photoinduced and quenched metastable states in a Prussian blue analog

Miho Itoi,[1,2] Isabelle Maurin,[3] François Varret,[1] Franz A. Frye,[4] Daniel R. Talham,[4] Dmitry Chernyshov,[5] and Kamel Boukheddaden[1,*]

[1]*Groupe d'Etudes de la Matière Condensée, UMR 8635, CNRS-Université de Versailles Saint-Quentin-en-Yvelines, 45 Avenue des Etats Unis, 78035 Versailles, France*

[2]*Division of Physics, Institute of Liberal Education, Nihon University School of Medicine, 173-8610 Tokyo, Japan*

[3]*Laboratoire de Physique de la Matière Condensée, UMR 7643, CNRS-Ecole Polytechnique, Route de Saclay 91120 Palaiseau, France*

[4]*Department of Chemistry, University of Florida, Gainesville, Florida 32611-7200, USA*

[5]*Swiss-Norwegian Beam-Lines, European Synchrotron Radiation Facility, BP 220, 38048 Grenoble Cedex, France*

(Received 14 April 2013; revised manuscript received 1 August 2013; published 6 September 2013)

The structural aspects of the metastable states for $K_{0.32}Co[Fe(CN)_6]_{0.76}\cdot 3H_2O$ have been investigated by synchrotron x-ray powder diffraction. The title compound exhibits nonequilibrium high spin (HS) states of $Co^{II}(S = 3/2)$-$Fe^{III}(S = 1/2)$ configuration, induced by rapid cooling or photoexcitation from the low-temperature (LT) phase. By introducing a new local order parameter of *tilting angle* between cyanide-bridged Fe and Co-based octahedra, we discovered the existence of a precursor phenomenon triggering the collective instability during the thermal relaxation of the photoexcited (PX) state. Moreover, we introduced a methodology, based on the flow diagram studies, which allowed us to clearly distinguish the obtained metastable states through their strength of spin-lattice coupling, leading to various pathways in the phase space during the combined electroelastic relaxation process.

DOI: 10.1103/PhysRevB.88.094104 PACS number(s): 61.66.Fn, 75.40.Gb

I. INTRODUCTION

Cobalt-iron Prussian blue analogs (CoFe PBAs), of general formula $A_xCo[Fe(CN)_6]_y\cdot zH_2O$ (A = Na, K, Rb, Cs), have attracted considerable attention over the last few decades, since their photoswitchable character could potentially be utilized for applications in memory devices and magneto-optical switching.[1,2] Reversible photoswitching in bistable CoFe PBAs is provided by a charge-transfer induced spin transition (CTIST), $Co^{III}(S = 0)$-$Fe^{II}(S = 0) \leftrightarrow Co^{II}(S = 3/2)$-$Fe^{III}(S = 1/2)$, with concomitant structural transformation predominantly attributed to the Co-N bond stretching, by 0.19 Å,[3,4] upon high spin (HS) to low spin (LS) state change of Co atom. The research on the key parameters controlling the photoexcitation process in CoFe PBAs has become a major subject,[4,5] including active investigations of hidden states (multimetastability),[6–8] and observations of local structural modifications under irradiation.[3,9]

Generally, photoexcitation of photoswitchable molecular solids, such as spin-crossover (SC) complexes,[10] is obtained with an irradiation energy (∼1 eV) which far exceeds the activation energy (∼100 meV) between the two *stable* states of the switchable units. The excess energy is released to the system via electron-lattice coupling. When photoexcitation is performed at very low temperature, the excited nonequilibrium state may be trapped, producing various long-living spin and lattice metastable structures. Consequently, instead of the usual one-order parameter description, the system involves two or even more order parameters, which can be eventually coupled.

$K_{0.32}Co[Fe(CN)_6]_{0.76}\cdot 3H_2O$ is a typical example of such bistable molecular solids, in which CTIST can be triggered both by temperature and light irradiation.[1,11] In this compound, a rapid cooling from the high-temperature (HT) phase allows for an efficient trapping of the $Co^{II}(S = 3/2)$-$Fe^{III}(S = 1/2)$ active pairs. The quenched (Q) metastable HT phase exhibits magnetic order below 14 K.[1,11,12] The Q state undergoes a thermal relaxation at ∼160 K, and then the diamagnetic $Co^{III}(S = 0)$-$Fe^{II}(S = 0)$ pairs (LT state) are formed by CTIST. On the other hand, by slow cooling (∼1 K/min) from the HT state, the system reaches an intermediate (IM) phase, which is a biphasic state, consisting of a mixture of LT and Q-like states.[1,11] By red-light irradiation at low temperature, two different photoexcited states have to be considered depending on the initial state, either the LT state (LTPX) or the IM state (IMPX). These LTPX and IMPX states show magnetic ordering at 18 and 17 K, respectively.[1]

An identification of the structural differences between the several types (photo- and thermotrapped) of HS metastable states is a difficult task due to their disordered nature. However, some characteristic features have been detected in the thermal decay processes and therefore can be found in the descriptors of the average structure. In this paper we present the thermal evolution of Q and LTPX average structures as seen by synchrotron x-ray powder diffraction (XRPD). We also discuss the stability of the various metastable states together with correlations between order parameters identifying different regimes of structural response.

II. EXPERIMENTAL SECTION

The preparation of the $K_{0.32}Co[Fe(CN)_6]_{0.76}\cdot 3H_2O$ sample was described in Refs. 1 and 11. The synchrotron x-ray powder diffraction (XRPD) experiments were carried out at the Swiss-Norwegian Beamlines (station BM1A) at ESRF, France. The sample was sealed in a $\phi = 0.1$ mm Lindemann glass capillary and XRPD patterns were collected every 4 K, from 90 to 300 K, with 1 K/min temperature sweep rate using an Oxford cryostream nitrogen blower. Powder LaB_6 (NIST standard) was used to calibrate the wavelength,

sample-to-detector distance, beam center, and tilt angle of the image plate detector (MAR345). The XRPD data described in the present work correspond to two sets of experiments with incident x-ray wavelength of (1) 0.71140 Å and (2) 0.71830 Å. After 1.5 min exposure, the intensity distribution within the Debye-Scherrer rings appeared homogeneous. For the structural study of the LTPX phase, we used a laser diode system with $\lambda = 690$ nm (50 mW/cm^2) and an irradiation time of 1.5 h. Rietveld refinements were carried out using the FullProf suite of programs.[13]

Magnetic susceptibility was measured on the same sample batch. Full characterization was reported in Ref. 1. Two sets of XRPD measurements were carried out at several month intervals. To check a possible sample ageing, quenching of the high-temperature phase followed by thermal relaxation was monitored in the two series of experiments. Peak positions and intensities were in fair agreement for the two data sets indicating the absence of significant structural modifications upon sample storage.

III. RESULT AND DISCUSSION

The crystal structure of $K_{0.32}Co[Fe(CN)_6]_{0.76}\cdot 3H_2O$ is NaCl type with a three-dimensional Co-NC-Fe network. The space group is $Fm\bar{3}m$ (No. 225). According to neutron diffraction studies,[14] water molecules occupy three independent *Wyckoff* positions: one is ligand water (H_2O_L), coordinated to Co atoms (24*e* site), while the two others are zeolitic water (H_2O_Z), with a large spatial distribution, either in the center of the empty suboctants (H_2O_{Z1}, 8*c* site) or slightly off-centered at (x, x, x) due to hydrogen bonding with H_2O_L (H_2O_{Z2}, 32*f* site). Detailed zeolitic water positioning was also reported in Ref. 15. As the electronic densities of K and H_2O_{Z1} largely overlap in the average crystal structure, we limit the present structural model to a single type of zeolitic water molecule (H_2O_{Z2} at 32*f*), in order to decrease the number of correlations in the refinement. Thus, the static positional disorder of zeolitic water is artificially taken into account in the thermal displacement factor. The existence of hydrogen bonding within the crystal, in addition to vacancies on $Fe(CN)_6$ sites, probably yields an additional structural degree of freedom associated with a slight change of Fe-Co distance due to a bending of the Fe-CN-Co bridges [5(b)]. Therefore, anisotropic atomic displacement parameters (ADPs) for C, N, and O_1 atoms are introduced to parametrize a smearing of electron density due to the thermal motion or a disorder. The anisotropy of ADPs represents a tilting of rigid [$Fe(CN)_6$] octahedra. This idea is based on previous structural studies related to zeolitic iron cyanides.[16] In the refinement, the tensor of displacement parameters is set to the diagonal form U_{ii} ($i = 1$–3), according to the crystal symmetry. ADPs along the cubic edge, i.e., U_{11}(C) and U_{11}(N) are assumed to be equivalent due to the tight C≡N bonding, yielding only short displacements. Furthermore, the constraint $U_{11}(O_L) = U_{11}(N)$ is used since N and O_1 are both coordinated to Co atoms. As a consequence, the electronic distribution for the C and N atoms is modeled as *disklike* in the *bc* plane ($U_{22} = U_{33}$) as shown in Fig. 1(a).

The x-ray diffraction pattern at 295 K and the corresponding Rietveld refinement are shown in Fig. 1(b). The experimental profile was collected over a large Q range ($Q < 7.9$ Å^{-1}), so

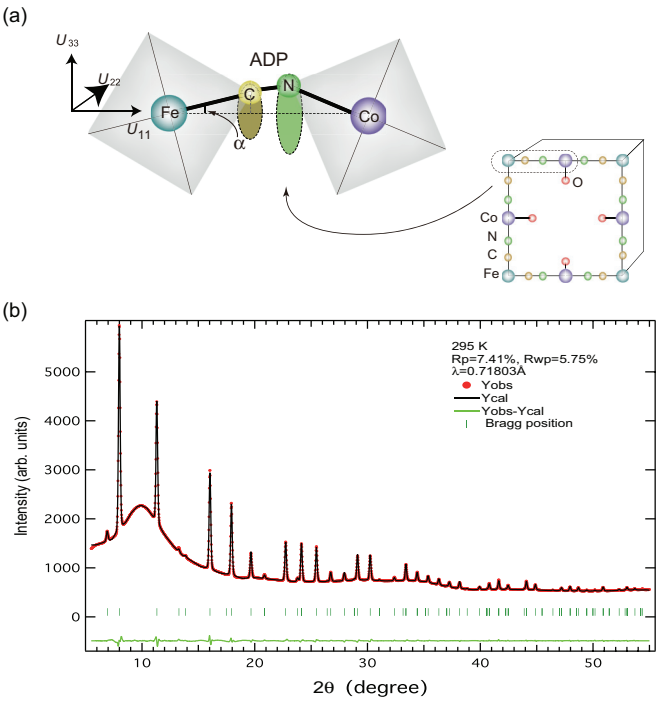

FIG. 1. (Color online) (a) Scheme of the tilted $Fe(CN)_6$ and $CoN_{6-x}O_x$ octahedra and associated anisotropic atomic displacements. (b) Synchrotron x-ray diffraction pattern of $K_{0.32}Co[Fe(CN)_6]_{0.76}\cdot 3H_2O$ at room temperature (red filled circles) and calculated profile (solid line) in the 2θ interval 5.5°–55°. The green line in the bottom of the figure is the difference between the calculated and the measured patterns. The wavelength corresponds to $\lambda = 0.71803$ Å.

as to accurately estimate the site occupancies and the thermal displacement factors of the various atoms. The wavelength corresponds to $\lambda = 0.71803$ Å. Refinement parameters are $R_p = 7.49\%$, $R_{wp} = 5.76\%$, and $R_e = 0.42\%$. Note that the thermal displacement factors of K and O_{Z1}, which occupy the same crystallographic position, were constrained to be equal in order to decrease the number of refined parameters. The refined atomic positions and thermal factors obtained by Rietveld analysis are listed in Table I. The lattice parameter at 295 K is 10.30626(10) Å. The Co-N and Fe-C bond lengths are 2.0779(20) and 1.9296(19) Å, respectively. These values are typical of Co^{II}($S = 3/2$, HS) and Fe^{III}($S = 1/2$, LS) species, and are in good agreement with EXAFS data [3,5(b),9], 2.094 Å (Co-N) and 1.915 Å (Fe-C). Extensions of the electron density for C and N perpendicular to the Fe-Co bond is mainly due to a tilting of $CoN_{6-x}O_x$ and $Fe(CN)_6$ octahedra. This tilting corresponds to dynamic or static disorder, which keeps the average tilting angle equal to zero in order to maintain the average $Fm\bar{3}m$ symmetry [8(a)]. However, the mean square value of the tilting angle is not zero, as well as its root mean square (rms) value. We estimate the rms tilting angle $\langle\alpha\rangle$ on the basis of simple geometric calculations, using the values of atomic thermal displacement parameter U_{33}, normal to the Fe-Co bond d(Fe-C), as follows:

$$\langle\alpha\rangle = \tan^{-1}\left(\frac{\sqrt{U_{33}(\mathrm{C})}}{d(\mathrm{Fe\text{-}C})}\right). \quad (1)$$

TABLE I. Structural parameters of the title compound $K_{0.32}Co[Fe(CN)_6]_{0.76}\cdot 3H_2O$ at room temperature with anisotropic thermal factors obtained by Rietveld analysis.

Atom	x	y	z	U_{eq}	U_{11}	U_{22}	U_{33}	Occ	Wyckoff
Co	0	0	0	0.0113(3)				1.0	4*a*
Fe	1/2	1/2	1/2	0.0113(3)				0.76	4*b*
C	0.31278(18)	0	0		0.0152(13)	0.036(2)	0.036(2)	4.6	24*e*
N	0.20163(19)	0	0		0.0152(13)	0.089(3)	0.089(3)	4.6	24*e*
K/O_{Z1}	1/4	1/4	1/4	0.156(10)				0.32	8*c*
O_L	0.2085(7)	0	0		0.0152(13)	0.0152(13)	0.0152(13)	1.4	24*e*
O_{Z2}	0.2867(19)	0.2867(19)	0.2867(19)	0.156(10)				1.6	32*f*

From the structural parameters of Table I, we estimated the rms rotation of the $[Fe(CN)_6]$ octahedra as $\langle\alpha\rangle = 5.6(2)^\circ$ at 295 K, which leads to the rms value for ∠C-N-Co = 166.3(3)°. An ordering of rotations would result in symmetry lowering; the angular deformation may therefore be considered as an order parameter. Note that the RMS ∠C-N-Co value calculated for this disordered $Fm\bar{3}m$ structure is close to the ordered angular deformations of other PBA compounds with $P21/n$ space group, $K_2Co[Fe(CN)_6]$ (∠C-N-Co = 172°)[17] and A_2Mn^{II} $[Mn^{II}(CN)_6]$ (A = K and Rb) (∠C-N-Mn = 173° and 177°, respectively).[18] Similar analyses were performed for the Q and LTPX metastable states. The corresponding plots are shown in Fig. 2 and the refined parameters are summarized in Tables II and III. XRPD patterns of the Q and LTPX states were recorded at 90 K in the range $5^\circ < 2\theta < 43^\circ$, with $\lambda = 0.71140$ Å. Obtained R factors were $R_p = 8.40\%$, $R_{wp} = 5.77\%$, and $R_e = 0.94\%$ for the Q phase and $R_p = 8.95\%$, $R_{wp} = 6.23\%$, and $R_e = 0.89\%$ for the LTPX phase. The Co-N [d(Co-N)] and Fe-C [d(Fe-C)] bond distances were also estimated, yielding the following values: d(Co-N) = 2.0709(20) Å and d(Fe-C) = 1.9235(19) Å for Q, d(Co-N) = 2.099(5) Å and d(Fe-C) = 1.917(4) Å for LTPX. Tilting angles were estimated to be $\langle\alpha\rangle_Q \sim 7.2^\circ$ and $\langle\alpha\rangle_{LTPX} \sim 7.1^\circ$ at ∼90 K, respectively These deviations from linear Fe-CN-Co entities should strongly affect magnetic superexchange interactions, and might be responsible for the local fluctuations of anisotropy from which may originates the spin-glass character of the Q phase.[12] The temperature dependencies of the lattice parameter a and those of $\langle\alpha\rangle$ and ∠C-N-Co angles for the LTPX and Q states are shown in Figs. 3(b) and 3(c).

It is important to note that the Rietveld analyses were restricted to single-phase patterns, i.e., up to temperatures of 145–152 K. At higher temperatures, HS(HT)-like and LS(LT)-like phases coexist, with large and small lattice parameter values, respectively. Then, asymmetric line shapes and peak overlapping largely influence data modeling and make any Rietveld analysis unreliable. Nevertheless, peak positions were sufficiently well defined to extract lattice parameter values through LeBail analyses [Fig. 3(a)].

In the LTPX phase, the lattice parameter starts to decay at ∼130 K, and a dramatic change is observed at ∼150 K, where the LTPX phase relaxes toward the LT state with a lattice constant of 9.960(7) Å. At the local level, the tilting angle value $\langle\alpha\rangle$ starts from ∼7.0°, begins to increase at ∼110 K and saturates at ∼8.4° around 140 K. The $\langle\alpha\rangle(T)$ curve is sigmoidal in shape thus indicating a dominant cooperative contribution from the rotational disorder rather than from phonons, the latter contribution dominating in the majority of compounds would result in a linear increase with the temperature.[19] Both temperature dependencies of $\langle\alpha\rangle$ and ∠C-N-Co exhibit an inflection point at ∼123 K. In addition, the lattice parameter of the Q phase starts to decay at 150 K, and undergoes a dramatic change around 160 K, where the structure shows

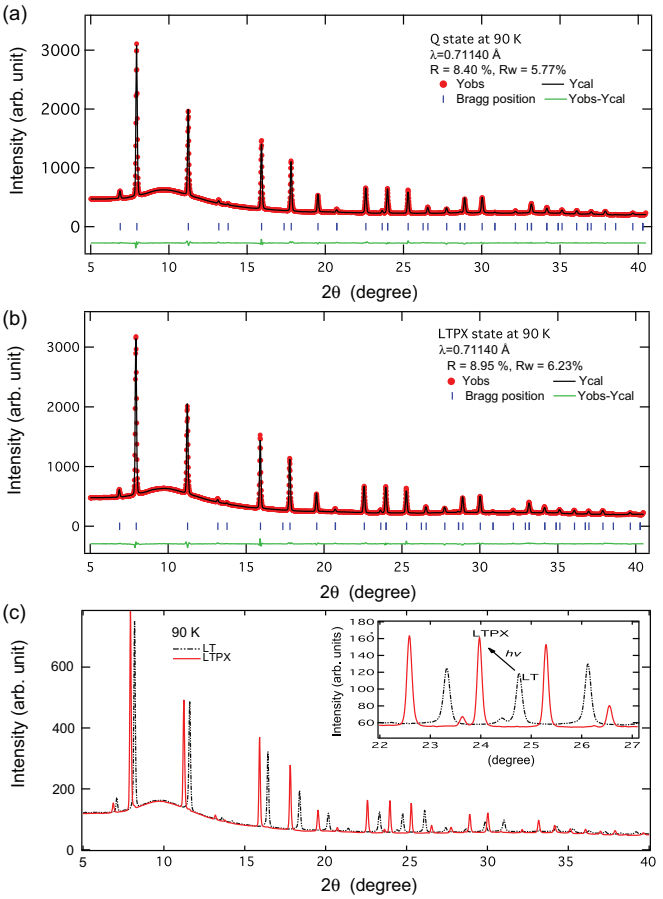

FIG. 2. (Color online) Synchrotron x-ray diffraction pattern (red filled circles) of $K_{0.32}Co[Fe(CN)_6]_{0.76}\cdot 3H_2O$ measured at 90 K in (a) the Q and (b) the PXLT state with calculated profiles (black solid line) in the 2θ interval 5°–41°. The green line in the bottom represents the difference between the experimental and calculated pattern. The wavelength corresponds to $\lambda = 0.71140$ Å. (c) X-ray diffraction pattern in LT (black dotted lines) and LTPX phase (red line) at 90 K. By red right irradiation, the LT phase is converted into the LTPX phase characterized by a large volume change (see inset)

TABLE II. Structural parameters of the title compound $K_{0.32}Co[Fe(CN)_6]_{0.76}\cdot 3H_2O$ for quench state at 90 K.

Atom	x	y	z	U_{eq}	U_{11}	U_{22}	U_{33}	Occ	Wyckoff
Co	0	0	0	0.0084(3)				1.0	4*a*
Fe	1/2	1/2	1/2	0.0084(3)				0.76	4*b*
C	0.31287(18)	0	0		0.0120(18)	0.057(5)	0.057(5)	4.6	24*e*
N	0.20147(19)	0	0		0.0120(18)	0.068(4)	0.068(4)	4.6	24*e*
K/O_{Z1}	1/4	1/4	1/4	0.078(4)				0.32	8*c*
O_L	0.2057(8)	0	0		0.0120(18)	0.0120(18)	0.0120(18)	1.4	24*e*
O_{Z2}	0.3007(5)	0.3007(5)	0.3007(5)	0.078(4)				1.6	32*f*

the largest thermal rate change during the relaxation process [Fig. 3(a)]. In contrast, the associated temperature dependence of the tilting angle $\langle\alpha\rangle_Q$ shows an almost linear increase ($\angle$C-N-Co decrease) from $\langle\alpha\rangle_Q = 7^\circ$ to 8° in the 90–150 K temperature interval, representative of the gradual increase of the ADPs parameters U_{33}(C) and U_{33}(N).

In Fig. 3(d) we present the temperature dependencies of bond lengths Fe-C and Co-N in the LTPX and Q phases. Clearly no important change is detected in the LTPX phase, while a slight variation appears in the Q phase, from 130 K, on heating. Consequently, we kept the structural symmetry of $Fm\bar{3}m$ at all phases in the structural analysis, because clear symmetry change is not observed in this compound.

Let us discuss briefly the possible effect of intrinsic disorder of ligand waters. The ligand water is a thermal molecule bonded to Co atom, and it complements the vacancies of $Fe(CN)_6$. Here we treat the thermal factor of the ligand water molecule as isotropic (see Table I), which means that the thermal molecule is free from twist and/or buckling (tilting) by the neighbor octahedron. The thermal vibration (moving) of ligand water is distinguished by the ADP of $Fe(CN)_6$ in our structural model. The discrimination from spatial disorder effect can be confirmed by the temperature dependencies of the displacements U_{33} and U_{11} for C and N (and O_L), U_{eq} for Co and Fe [see Figs. 3(e) and 3(f)]. $U(O_1)$ [$= U_{11}$(C) and U_{11}(N)] and U(Fe) show linear increase in the temperature range of 90–140 K, then they are largely changed at the vicinity (starting point) of thermal relaxation. Furthermore, the anisotropic precursor structural transformation at 123 K in LTPX is also found in the result of temperature dependencies of FWHM of (h, k, l) diffraction peaks. The diffraction peaks become narrower at around 125 K, whose value is in good agreement with the inflexion point of the tilting angle. The behavior shows (h, k, 0) dependencies. This behavior does not relate to an intrinsic disorder of a ligand water molecule, because this kind of disorder probably occurs averagely in the whole crystal.

On the other hand, $\langle\alpha\rangle$ is a local structural parameter, however this parameter relates to the coherent structural change such as observation of FWHM narrowing. So, the tilting angle can express very small (microscopic) and coherent structural change which we cannot clearly observe in macroscopic techniques, like heat capacity or/and magnetic measurements. The decay process of nonequilibrium states in $K_{0.32}Co[Fe(CN)_6]_{0.76}\cdot 3H_2O$ can be understood in more detail by introducing flow diagrams, which plot the evolution of the system in the order-parameter space, for instance the HS fraction ($\chi_M T$) vs any of the structural parameters derived from the XRPD measurements. χ_M represents the molar susceptibility and T is the temperature. Note that temperature dependent magnetization and XRPD measurements were recorded at the same sweep rate, 1 K min^{-1}. In Fig. 4(a) we show the correlation between the $\chi_M T$ and the lattice parameter a. It is generally expected that the lattice parameter linearly couples to the order parameter (magnetic moment) for spin conversion due to elastic interactions, which result in a bilinear coupling between the spin state and the lattice parameter, in a first approximation. However, this simple view is valid only at equilibrium and high temperature. The things become much more complex when we study nonequilibrium states (metastable states) at low temperature. There, higher order coupling terms and other origins of nonlinearities (anharmonicity, for example) may affect the potential energy landscape, which becomes much more complex. In addition, the difference of time scales of the various operating order parameters will be emphasized in the low temperature region where the system dynamics slows down. This leads to well separated thermal relaxation regimes when the order parameters are weakly coupled, or to interferences when the coupling is strong. Thus, for the LTPX phase, three successive regimes characterized by different

TABLE III. Structural parameters of the title compound $K_{0.32}Co[Fe(CN)_6]_{0.76}\cdot 3H_2O$ for LTPX state at 90 K.

Atom	x	y	z	U_{eq}	U_{11}	U_{22}	U_{33}	Occ	Wyckoff
Co	0	0	0	0.0099(3)				1.0	4*a*
Fe	1/2	1/2	1/2	0.0099(3)				0.76	4*b*
C	0.3135(4)	0	0		0.019(2)	0.059(5)	0.059(5)	4.6	24*e*
N	0.2042(5)	0	0		0.019(2)	0.067(4)	0.067(4)	4.6	24*e*
K/O_{Z1}	1/4	1/4	1/4	0.082(4)				0.32	8*c*
O_L	0.2008(15)	0	0		0.019(2)	0.019(2)	0.019(2)	1.4	24*e*
O_{Z2}	0.3003(6)	0.3003(6)	0.3003(6)	0.082(4)				1.6	32*f*

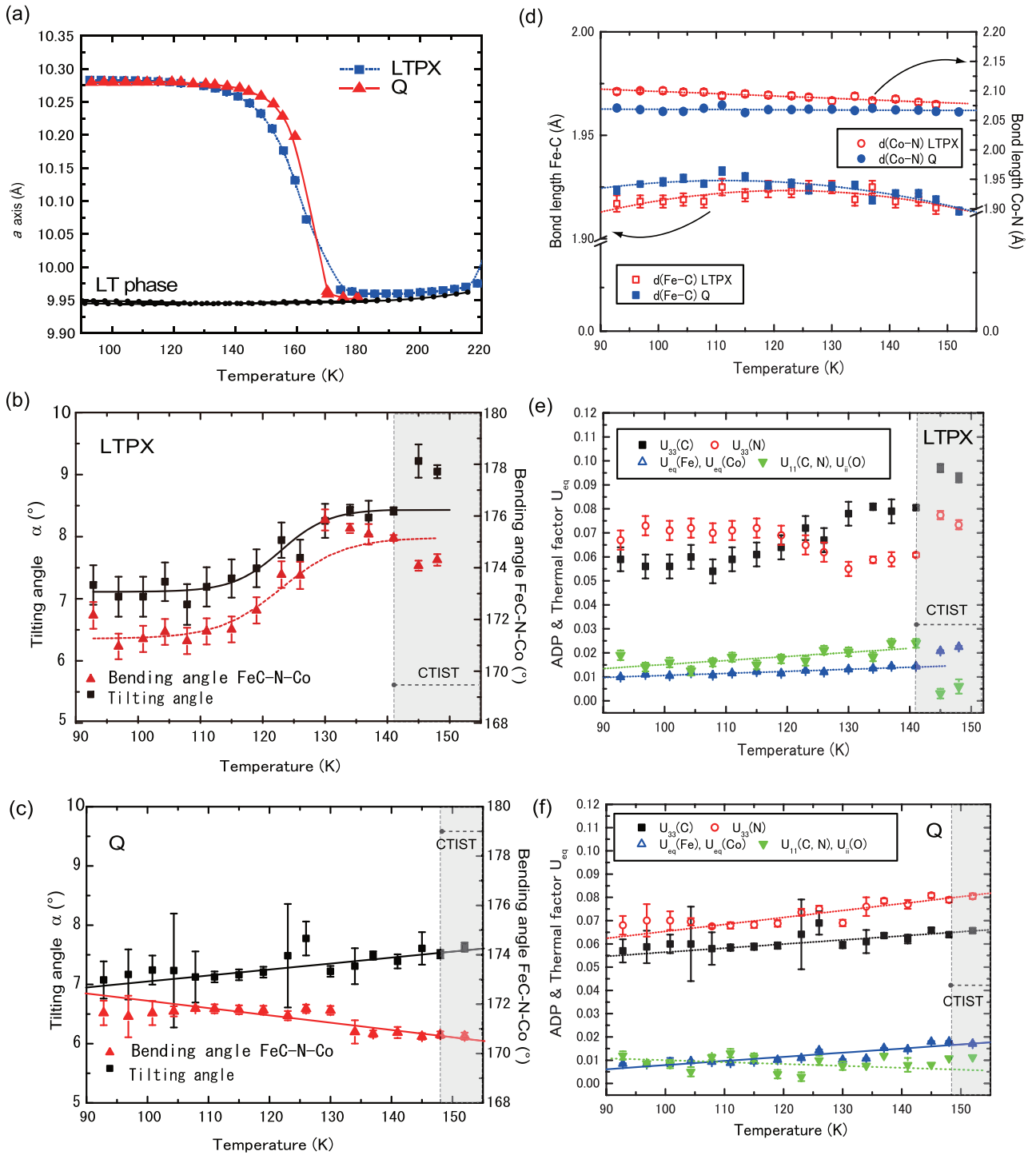

FIG. 3. (Color online) (a) Change in the lattice parameter a upon thermal relaxation from HS to LS states ($90 < T < 220$ K) for both LTPX and Q phases, as derived from LeBail analysis. (b) and (c) Corresponding thermal behavior of the tilting angle $\langle\alpha\rangle$ and of the ∠C-N-Co angle between $Fe(CN)_6$ and $CoN_{6-x}O_x$ octahedra for the LTPX and Q states, respectively (d) Temperature dependencies of Fe-C and Co-N bond lengths in LTPX and Q states. (e) and (f) Respective temperature dependent isotropic thermal factor U and each ADP parameters (C, N) for the LTPX and Q states.

values of the slope $\Delta a/\Delta\chi_M T$ are observed. In the first regime (A), the lattice parameter remains almost unchanged while the magnetic signal dramatically decreases, with $\Delta a/\Delta\chi_M T \sim 0.011$ Å mol emu^{-1}. This initial regime (90–112 K) concerns only 15% of the total $\chi_M T$ signal, and is assigned to the rapid CTIST of the inhomogeneous part of photoexcited domains, located at the interface between the saturated photoexcited area and LT phase. The second regime (B), observed in the interval 117–141 K, is similar to the first one, but it is ascribed to the CTIST process of bulky photoexcited species, and it is

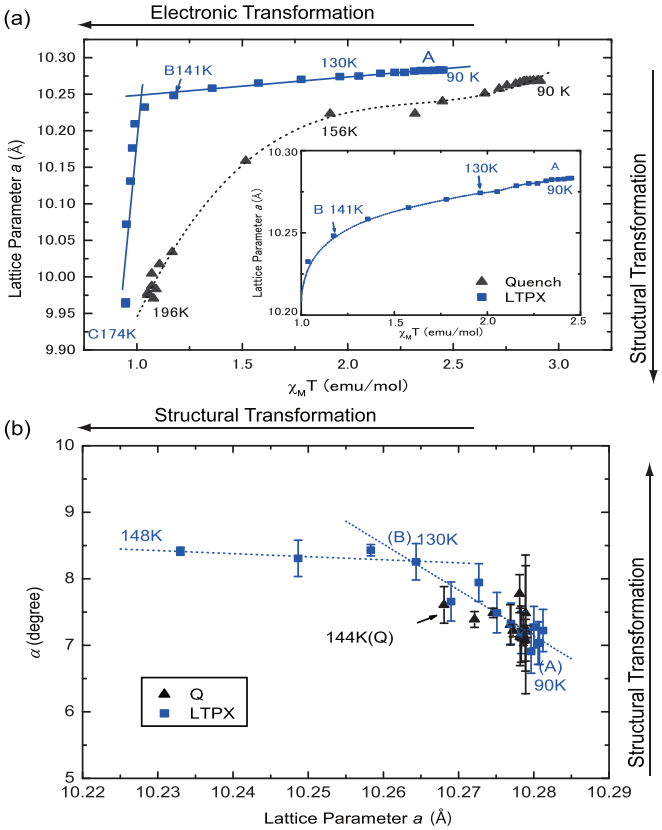

FIG. 4. (Color online) Flow diagrams of (a) $\chi_M T$ vs lattice parameter a. The labels A, B, and C stand for the three relaxation regimes discussed in the main text. (b) Correlation between $\langle\alpha\rangle$ and a parameters.

a collective process. Indeed, magnetization decreases rapidly, $\Delta a/\Delta\chi_M T \sim 0.036$ Å mol emu^{-1}, with a relatively small change in lattice constant ($\Delta a/a \sim 0.5\%$). Thus, regimes A and B are strictly related to the electronic CTIST process, with increasing LS fraction; however, the Fe-C and Co-N bond lengths remain typical of HS state: 1.922(3) and 2.090(5) Å, respectively at 141 K for the LTPX phase. The third regime (C) starts above 141 K with a dramatic structural transformation, $\Delta a/\Delta\chi_M T \sim 2.940$ Å mol emu^{-1}, as the lattice parameter relaxes to the LT-phase value. This kind of well decoupled relaxation regimes between the spin and the lattice has also been observed in the SC complex $[FeH_2L_2\text{-}Me](ClO_4)$.[20] The evolution of the Q phase strongly contrasts with that of the LTPX phase [Fig. 4(a)]. The variations of the lattice and electronic subsystems are obviously nonlinearly coupled during the whole thermal relaxation process, at variance with the LTPX phase. Indeed, the steep character of the electronic CTIST is not extensively observed and the crossover between the two regimes is not clear, although well characterized by two $\Delta a/\Delta\chi_M T$ values of ~0.056 and ~0.393 Å mol emu^{-1}. The data of the new local order parameter $\langle\alpha\rangle$, obtained between 90 and 148 K, made possible a detailed investigation of the structural relaxation process. In Fig. 4(b) we show the flow diagram of the system in $\langle\alpha\rangle$-a coordinates. The temperature range has been restricted to single-phase HS-like diffraction patterns. Interestingly, for the LTPX phase, the flow diagram shows a crossover at ~130 K, which evidences the presence of two successive regimes, characterized by major changes in $\langle\alpha\rangle$ and in a, below and above 130 K, respectively. The $\langle\alpha\rangle$ variation precedes the lattice parameter variation, and this suggests that the local distortion, at the molecular level, triggers the macroscopic instability.

IV. CONCLUSION

In summary, we have analyzed the structural relaxation of the LTPX and Q phase of $K_{0.32}Co[Fe(CN)_6]_{0.76}\cdot 3H_2O$ by XRPD. We evaluated the $\langle\alpha\rangle$ and ∠C-N-Co bending angles from ADP parameters. $\langle\alpha\rangle$ is found to be a relevant parameter allowing the estimation of the intrinsic degree of structural disorder, at the molecular level. The spin and lattice dynamics of thermal relaxation was analyzed by using various flow diagrams, between the macroscopic ($\chi_M T$) and the microscopic structural parameters a and $\langle\alpha\rangle$. The metastable HS phase of LTPX and Q were clearly differentiated by the strength of the coupling between electronic CT and lattice degrees of freedom. The electronic CTIST and structural transformation are weakly coupled for the LTPX state, and their main variations occur successively, while for the Q state the coupling is strong and nonlinear; the relaxation proceeds through a joint change of both degrees of freedom over a small temperature interval. The variation of the Fe-CN-Co bond bending has been observed as precursory collective lattice change. The correlation flow diagrams proposed in this paper gave new insights to the relaxation dynamics of the thermally and photoinduced metastable HS states.

ACKNOWLEDGMENTS

This work was financially supported by CNRS, Versailles University, Region Ile-de France, European Union Network of Excellence MAGMANet (Contract No. NMP3-CT-2005-515767-2) and partially supported by the US National Science Foundation through Grants No. DMR-0453362 and No. DMR-1005581 (DRT). The authors acknowledge the ESRF for provision of synchrotron x-ray beam time.

*itoi.miho@nihon-u.ac.jp; kbo@physique.uvsq.fr

[1]C. Chong, M. Itoi, K. Boukheddaden, E. Codjovi, A. Rotaru, F. Varret, F. A. Frye, D. R. Talham, I. Maurin, D. Chernyshov, and M. Castro, Phys. Rev. B **84**, 144102 (2011).

[2]O. Sato, T. Iyoda, A. Fujishima, and K. Hashimoto, Science **272**, 704 (1996); O. Sato, Y. Einaga, T. Iyoda, A. Fujishima, and K. Hashimoto, J. Electrochem. Soc. **144**, L11 (1997); H. Tokoro, S.-i. Ohkoshi, and K. Hashimoto, Appl. Phys. Lett. **82**, 1245 (2003); D. A. Pejaković, J. L. Manson, C. Kitamura, J. S. Miller, and A. J. Epstein, Polyhedron **20**, 1435 (2001); K. Kato, Y. Moritomo, M. Takata, M. Sakata, M. Umekawa, N. Hamada, S. Ohkoshi, H. Tokoro, and K. Hashimoto, Phys. Rev. Lett. **91**, 255502 (2003);

T. Matsuda, H. Tokoro, K. Hashimoto, and S. Ohkoshi, Dalton Trans. **2006**, 5046 (2006); S.-i. Ohkoshi, T. Iyoda, A. Fujishima, and K. Hashimoto, Phys. Rev. B **56**, 11642 (1997); S.-i. Ohkoshi, Y. Abe, A. Fujishima, and K. Hashimoto, Phys. Rev. Lett. **82**, 1285 (1999).

[3]T. Yokoyama, T. Ohta, O. Sato, and K. Hashimoto, Phys. Rev. B **58**, 8257 (1998).

[4]C. Cartier dit Moulin, F. Villain, A. Bleuzen, M. Arrio, P. Sainca-tavit, C. Lomenech, V. Escax, F. Baudelet, E. Dartyge, J. Gallet, and M. Verdaguer, J. Am. Chem. Soc. **122**, 6653 (2000).

[5]J.-D. Cafun, L. Londinière, E. Rivière, and A. Bleuzen, Inorganica Acta **361**, 3555 (2008); V. Escax, G. Champion, M.-A. Arrio, M. Zacchigna, C. Cartier dit Moulin, and A. Bleuzen, Angew. Chem. Int. Ed. **44**, 4798 (2005); A. Bleuzen, C. Lomenech, V. Escax, F. Villain, F. Varret, C. Cartier dit Moulin, and M. Verdaguer, J. Am. Chem. Soc. **122**, 6648 (2000); V. Escax, A. Bleuzen, C. Cartier dit Moulin, F. Villain, A. Goujon, F. Varret, and M. Verdaguer, *ibid.* **123**, 12536 (2001).

[6]N. Shimamoto, S.-i. Ohkoshi, O. Sato, and K. Hashimoto, Inorg. Chem. **41**, 678 (2002).

[7]H. Hanawa, Y. Moritomo, and J. Tateishi, J. Phys. Soc. Jpn. **10**, 2759 (2004).

[8]I. Maurin, D. Chernyshov, F. Varret, A. Bleuzen, H. Tokoro, K. Hashimoto, and S.-i. Ohkoshi, Phys. Rev. B **79**, 064420 (2009); S. Gawali-Salunke, F. Varret, I. Maurin, C. Enachescu, M. Malarova, K. Boukheddaden, E. Codjovi, H. Tokoro, S. Ohkoshi, and K. HashimotoJ. Phys. Chem. B **109**, 8251 (2005); J. Lejeune, J.-D. Cafun, G. Fornasieri, J.-B. Brubach, G. Creff, P. Roy, and A. Bleuzen, Eur. J. Inorg. Chem. **2012**, 3980 (2012).

[9]T. Yokoyama, M. Kiguchi, T. Ohta, O. Sato, Y. Einaga, and K. Hashimoto, Phys. Rev. B **60**, 9340 (1999).

[10]S. Pillet, V. Legrand, M. Souhassou, and C. Lecomte, Phys. Rev. B **74**, 140101(R) (2006); Y. Ogawa, S. Koshihara, K. Koshino, T. Ogawa, C. Urano, and H. Takagi, Phys. Rev. Lett. **84**, 3181 (2000).

[11]J.-H. Park, F. Fry, N. E. Anderson, D. M. Pajerowski, Y. D. Huh, D. R. Talham, and M. W. Meisel, J. Magn. Magn. Mater. **310**, 1458 (2007).

[12]D. M. Pajerowski, V. O. Garlea, E. S. Knowles, M. J. Andrus, M. F. Dumont, Y. M. Calm, S. E. Nagler, X. Tong, D. R. Talham, and M. W. Meisel, Phys. Rev. B **86**, 054431 (2012).

[13]J. Rodriguez-Carvajal, Physica B **192**, 55 (1993); http://www.ill.eu/sites/fullprof/index.html.

[14]F. Herren, P. A. Ludi, and W. Haelg, Inorg. Chem. **19**, 956 (1980); H. J. Buser, D. Schwarzenbach, W. Petter, and A. Ludi, *ibid.* **16**, 2704 (1977).

[15]J. E. Kim, K. Kato, M. Takata, T. Shibata, and Y. Moritomo, Phys. Rev. B **79**, 132105 (2009).

[16]E. Garnier, P. Gravereau, and A. Hardy, Acta Crystallogr. Sect. B **38**, 1401 (1982); P. Garvereau, E. Garnier, and A. Hardy, *ibid.* **35**, 2843 (1979); A. L. Goodwin, K. W. Chapman, and C. J. Kepert, J. Am. Chem. Soc. **127**, 17980 (2005); A. E. Phillips, G. J. Halder, K. W. Chapman, A. L. Goodwin, and C. J. Kepert, *ibid.* **132**, 10 (2010); T. Matsuda, J. E. Kim, K. Ohoyama, and Y. Moritomo, Phys. Rev. B **79**, 172302 (2009).

[17]K. H. Hallimeier, S. Sauter, and R. Szargan, Inorg. Chem. Commun. **4**, 153 (2001).

[18]J.-H. Her, P. W. Stephens, C. M. Kareis, J. G. Moore, K. S. Min, J. Park, G. Bali, B. S. Kennon, and J. S. Miller, Inorg. Chem. **49**, 1524 (2010).

[19]B. T. M. Willis and A. W. Pryor, *Thermal Vibrations in Crystallography* (Cambridge University Press, Cambridge, 1975).

[20]H. Watanabe, N. Bréfuel, S. Mouri, J.-P. Tuchagues, E. Collet, and K. Tanaka, Eur. Phys. Lett. **96**, 17004 (2011).